Hindawi
Advances in Civil Engineering
Volume 2021, Article ID 4256740, 9 pages
https://doi.org/10.1155/2021/4256740

Research Article

Research on the Influence of Weak Interlayer in Open-Pit Slope on Stability

Zhong Shuheng and Miao Yinjun

School of Energy and Mining Engineering, China University of Mining & Technology (Beijing), Beijing 100083, China

Correspondence should be addressed to Miao Yinjun; miaoyinjun@yeah.net

Received 3 June 2021; Accepted 30 June 2021; Published 8 July 2021

Academic Editor: Dezhong Kong

The weak interlayer in the slope meets with water threatening the overall stability of the slope. Sequestration location of the weak layer has an impact on the stability of the slope. Based on this, taking the south-side slope of Fushun West Open-Pit Mine as the background, the limit equilibrium method was used to study the influence of different depths and dip angles of weak interlayers on the factor-of-safety and sliding mode of the slope. After analyzing the effect, a bottom friction experiment was conducted to verify the theoretical results. The research results show that, as the buried depth of the weak layer becomes larger and the dip angle becomes smaller, the safety factor of the slope increases. Dip angle and depth both affect the sliding mode of the slope. This can provide a reference for study of the influence mechanism of weak interlayer on slope stability in multi-weak-layer slopes.

1. Introduction

Slope landslide is one of the three natural disasters. There are about 35,000 instability accidents due to weak interlayers in slopes ever year in China. These accidents pose a serious threat to the national property and people's lives [1].

In reality, the geological structure of the slope is complex, usually containing more than one weak interlayer. Studying which weak interlayer has the greatest impact on slope stability and the reasons are of great significance to the prevention and control of landslides.

Sloan [2] analyzed the slope with weak interlayer and verified that the weak interlayer is the main factor controlling the slope landslide. Li et al. [3] conducted a large-scale geomechanical model experiment to study the influence of rainfall infiltration on the slope characters. Liu et al. [4] studied the influence of the hydrological characteristics of the fracture zone composed of clay minerals on the slope stability. Li [5] studied the potential slip surface of the representative section of the southern slope of Fushun West Open-Pit Mine and determined that the potential slip surface is the weak interlayer in the slope. Sun and Li [6] studied open-pit mine slope stability based on improved TOPSIS method. In summary, as for research on the weak interlayers in slope, domestic scholars have focused on the changes in the mechanical properties of weak interlayers after being softened by water. However, there are few studies on the influence of the location of the softened weak layer on the overall stability and sliding mode of the slope. In this paper, the influence of the buried depth and dip angle of the weak layer on the slope stability and sliding mode is analyzed based on the background of the south slope of Fushun West Open-pit Mine. Then, a similar model experiments is conducted to validate the analysis results.

2. Influence of Weak Interlayer on Slope Stability and Sliding Mode

2.1. Mechanism of Weak Interlayer Softening. The weak interlayer is rich in clay minerals and has strong expansibility when exposed to water, which greatly reduces the shear strength of the weak interlayer [7–9]. According to the unsaturated soil strength theory [10,11], there is the following relationship between soil shear strength and matrix suction:

$$\tau_f = c' + (\sigma - u_\alpha)\tan\phi' + (u_\alpha - u_w)\tan\phi^b, \quad (1)$$

where τ_f is the shear strength, c' is the effective cohesion, σ is the normal stress, u_α is the atmosphere pressure, u_w is the

pore water pressure, $u_\alpha - u_w$ is the matrix suction, ϕ' is the friction angle in saturated state, and ϕ^b is the friction angle that varies with suction.

It can be seen from formula (1) that there is a linear function relationship between the shear strength of the weak interlayer and the suction force of the matrix. When the water content of the weak layer increases, the pore water pressure will increase, the matrix suction will decrease, and the shear strength will decrease.

2.2. Limit Equilibrium Analysis of Weak Layer Affecting Slope Stability. The model used in this paper comes from the E1200 section of the south slope of the Fushun West Open-Pit Mine. The stratigraphic composition is mainly Archean granite-gneiss, strongly weathered basalt, and weakly weathered basalt. There are 3 weak interlayers that can be proven. The simplified slope profile is shown in Figure 1. In Figure 1, the weak interlayers are marked as weak layer 1, weak layer 2, and weak layer 3 from top to bottom. Strongly weathered basalt is located above weak layer 1, and weakly weathered basalt is located between weak layer 1 and granite-gneiss.

By collecting, summarizing, and analyzing the rock and soil test results of previous projects, the rock mechanics parameters required for this calculation are shown in Table 1.

The factor-of-safety and factor-of-safety reduction ratio of the slope after softening of different weak interlayers are calculated based on the limit equilibrium method. The results are shown in Tables 2 and 3, respectively.

After comparing the safety factor reduction ratio of the three softened weak layers, obviously the softening of weak layer 1 has the greatest impact on the overall stability of the slope, followed by weak layer 2 and weak layer 3, the smallest in the model studied in this paper.

Judging from the sequestration location of the three weak layers in the slope, the buried depths and dip angles of the three weak layers are different, resulting in different degrees of influence on the slope of the three weak interlayers. The following uses the limit equilibrium method to calculate the safety factor of the slope to explore how the buried depth and dip angle of the weak interlayer affect the stability of the slope. Due to the dip angle, the buried depth of the weak layer has no definite value. In this paper, the vertical distance between the weak layer and the slope toe is defined as the buried depth of the weak interlayer. According to the above research model, the in situ burial depth of weak interlayer 1 is 40 m, and the base rock below the weak layer does not slide. The weathered basalt lies above the weak layer. The burial depth of the weak interlayer is increased by 20 m, and the safety factor of the slope and changing trend of slip surface is calculated by the limit equilibrium method. The results are shown in Table 4.

As shown in Table 4, when the buried depth of the weak interlayer increases while other factors remain unchanged, the safety factor of the slope gradually increases. The buried depth increases from the original 40 m to 80 m, and the sliding mode of the slope is sliding along the weak layer. When the buried depth is greater than 99 m, the safety factor is still increasing, but its sliding mode becomes shallow sliding along the slope surface. Therefore, when the dip angle is 23°, the buried depth of 99 m is the critical value for the change of the slope sliding mode.

According to the research model, the dip angle of weak interlayer 1 in the original position is 23°. Set the part below the weak layer as a non-slip bedrock, and the part above it as a strongly weathered basalt. Inclination angle increment is 3°. The results of the safety factor of the slope and changing trend of slip surface calculated by the limit equilibrium method are shown in Table 5.

It can be seen from Table 5 that when the dip angle of the weak interlayer decreases while other factors remain unchanged, the safety factor of the slope gradually increases. When the dip angle of the weak interlayer decreases from the original 23° to 9°, the sliding mode of the slope is sliding along the weak layer. When the dip angle of the weak interlayer is less than 8°, the safety factor is still increasing, but the sliding mode changes, and the sliding mode at this time becomes a shallow sliding along the slope.

Selecting the buried depth as 10 m, 70 m, and 140 m, when the slope is in the critical state of sliding along the shallow layer of the slope, the trend of the dip angle is shown in Table 6.

Taking the buried depth as the horizontal axis and the dip angle as the vertical axis, linear fitting is performed from the results obtained in Table 6. The law of the sliding mode of the slope is shown in Figure 2.

It can be seen from Figure 2 that the relationship between the buried depth and the dip angle is linear. The fitted straight line divides the first coordinate system into two parts. Take the value of the buried depth and dip angle at the upper left of the line; the slope will slide along the weak interlayer, and take the value of the buried depth and dip angle at the lower right of the line; the slope will slide shallowly, and the dividing line is the straight line obtained by linear fitting.

3. Bottom Friction Experiment

3.1. Design of the Experiment. When the three weak interlayers in the model are softened, it is the interlayer 1 that affects the stability of the slope most. Therefore, this section studies the influence of different dip angles and buried depths of weak layer 1 on slope stability and sliding mode to verify the calculation result of the limit equilibrium method.

Generalize the geological prototype. The generalized prototype is 1000 m long and 450 m high. Combined with the actual situation of the bottom friction test bench size: length × width × thickness = 1.0 m × 1.0 m × 0.05 m, the geometric similarity ratio of the simulation test is determined as $C1 = 1000 : 1$. The test model is shown in Figure 3.

Similar model experiment requires that the model is not only similar in geometry to the prototype, but also requires the physical quantities included in the test process to be similar to the prototype. This experiment uses a mixed material of sand, lime, and gypsum in different proportions to simulate the bedrock and basalt above it [12]. After

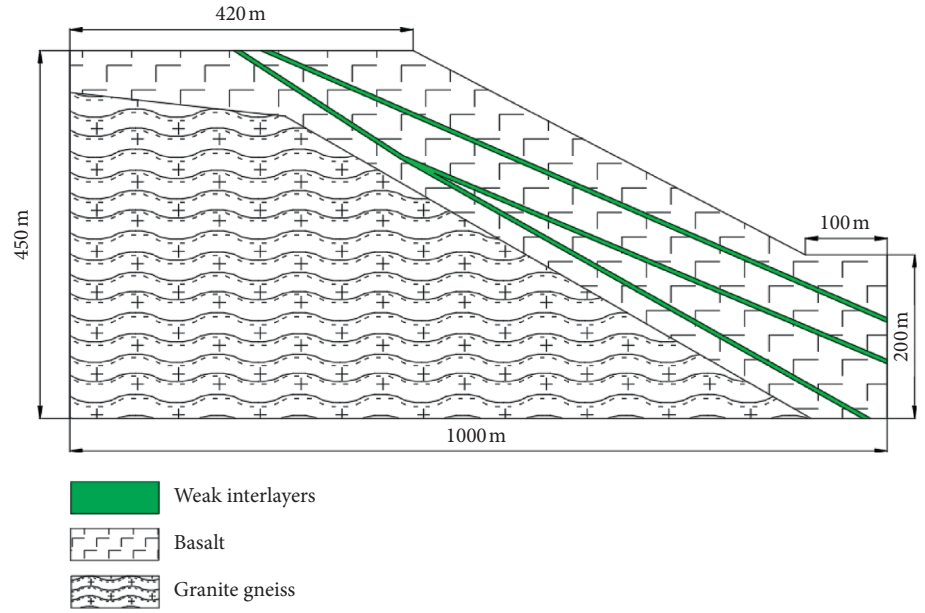

Figure 1: Simplified map of E1200 geological section.

Table 1: Rock mechanical parameters of each rock formation.

	Elastic modulus, E (MPa)	Cohesion, C (kPa)	Friction, Φ (°)	Poisson's ratio, ν	Volumetric weight, ρ (g·cm^{-3})
Granite gneiss	50000	30000	50	0.23	2.8
Weakly weathered basalt	11892	1810	37.2	0.26	2.6
Strongly weathered basalt	7824	1690	36.7	0.28	2.43
Weak interlayer 1	1076	220	21.6	0.32	2.4
Weak interlayer 2	1506	330	25.1	0.3	2.35
Weak interlayer 3	2500	450	30	0.3	2.0

Table 2: Factor-of-safety of the slope after softening of different weak layers.

	Factor-of-safety			
	Ordinary	Bishop	Janbu	Janbu generalized
Dry slope	1.068	1.100	1.068	1.109
Weak layer 1 softening	0.689	0.613	0.607	0.713
Weak layer 2 softening	0.950	0.971	0.912	1.048
Weak layer 3 softening	1.068	1.100	1.068	1.109

Table 3: Factor-of-safety reduction ratio of the slope after softening of different weak layers.

	Factor-of-safety reduction ratio			
	Ordinary (%)	Bishop (%)	Janbu (%)	Janbu generalized (%)
Weak layer 1 softening	35.48	44.27	43.16	35.71
Weak layer 2 softening	11.05	11.73	14.61	5.5
Weak layer 3 softening	0	0	0	0

Table 4: The relationship between buried depth of weak interlayer and slope stability.

Buried depth (m)	Safety factor	Sliding mode
40	1.069	Sliding along the weak layer
60	1.185	Sliding along the weak layer
80	1.314	Sliding along the weak layer
99	1.460	Shallow sliding on slope
120	1.461	Shallow sliding on slope

Table 5: The relationship between dip angle of weak interlayer and slope stability.

Dip angle (°)	Safety factor	Sliding mode
23	1.069	Sliding along the weak layer
20	1.158	Sliding along the weak layer
17	1.232	Sliding along the weak layer
14	1.307	Sliding along the weak layer
11	1.394	Sliding along the weak layer
8	1.460	Shallow sliding on slope

repeated tests, the percentage of each material is determined as shown in Table 7.

In order to verify the influence of the dip angle and buried depth of the weak interlayer on the stability and sliding mode of the rock slope, a total of four sets of experiments were designed: experiment 1—the weak layer is in the original position (23°, 44 mm); experiment 2—the dip angle decreases (8°, 44 mm); experiment 3—the buried depth increases (23°, 120 mm); and experiment 4— the dip angle and the buried depth both increase (29°, 100 mm).

3.2. Experiment Results and Analysis

3.2.1. Experiment 1: The Weak Layer Is in the Original Position (23°, 44 mm). When the slope is in the original state, the break process of the slope is shown in Figure 4.

Start the bottom friction machine; after running for 21 seconds (Figure 4(b)), the first crack L1 appeared at the foot of the basalt layer slope, the crack width was about 1 mm, and it penetrated the weak interlayer of the lower layer; after 23 seconds (Figure 4(c)), a new crack L2 appeared at the foot of the basalt slope, and a crack L3 appeared at the slope surface, which also penetrated the weak interlayer; after 26 seconds (Figure 4(d)), cracks L4, L5, and L6 appeared on the slope. At this time, the foot of the basalt in the upper part of the slope was completely destroyed; after 33 seconds (Figure 4(e)), the basalt part lost the support of the slope toe, and the entire basalt part was destroyed, sliding along the weak interlayer and cracks everywhere. At the end of the experiment (Figure 4(f)), the basalt layer sank 5 cm from the bedrock, and the overall displacement in the horizontal direction was 10 cm. The slope eventually broke. From the perspective of the break process of the slope, the toe of the slope was damaged first. The reason is that the toe of the slope is a stress concentration area. The toe of the slope was squeezed by the upper rock layer to cause shear failure. Secondly, cracks appeared on the surface of the slope, and the cracks gradually propagated upward from the middle and lower parts of the slope, and finally the slope appeared as a whole landslide. After the toe of the slope was damaged, the rock layer at the slope lost the support at the toe of the slope. The basalt layer in the middle and lower parts of the slope broke the connection with the rock layer in the middle and upper part under the action of gravity, resulting in damage. In short, after losing the support of the slope toe, the upper rock layer of the slope will be broken and destroyed step by step under the action of gravity. The slope eventually loses stability along the weak interlayer, and its sliding mode is in good agreement with the results of the limit equilibrium method.

3.2.2. Experiment 2: The Dip Angle Decreases (8°, 44 mm). When the dip angle of the weak interlayer is changed from the original 23° to 8°, and the other parameters remain unchanged, the photos of the slope at different moments are shown in Figure 5.

Start the bottom friction machine; after 15 seconds (Figure 5(b)), the shallow area on the top of the slope began to damage; after 23 seconds (Figure 5(c)), the scope of the slope top damage became larger, and the damage in the shallow area develops toward the middle part. At the same time, two cracks appeared on the slope surface. Crack L1 was arc-shaped, the entrance was at the top of the slope, and the exit was at the middle and upper part of the slope. Crack L2 is about 7 cm long and sloped upward along the slope. After 27 seconds (Figure 5(d)), a new crack L3 appeared on the sliding body; the crack was a vertical crack, about 5 cm long. In the end (Figure 5(e)), the shallow layer damage at the top of the slope has progressed to the middle layer, and the scope of damage has become larger. At the same time, a new crack L4 appeared on the upper sliding body, which is connected with L1 and L4 and divides the sliding body into four.

From the perspective of the break process, the break of the slope first occurred at the top of the slope. The slope top was damaged under the action of its own weight stress. With the rotation of the belt, the damage gradually develops to the slope surface. The cracks on the slope gradually increased, but the cracks did not extend to the interior of the slope. The slope was only partially damaged, and the whole slope remained stable. When the belt stopped rotating, the damage range at the top of the slope became larger than it was at the beginning, and the cracks on the slope increased. Generally speaking, the damage is shallow and local, and the slope does not slide along the weak interlayer. The slope remains stable as a whole.

3.2.3. Experiment 3: The Buried Depth Increases (23°, 120 mm). When the buried depth of the weak interlayer is changed from the original 40 m to 120 mm, and the other parameters remain unchanged, the photos of the slope at different moments are shown in Figure 6.

Start the bottom friction machine. After 20 seconds (Figure 6(b)), the model began to break. The first crack L1 appeared in the middle and upper parts of the slope. After 26 seconds (Figure 6(c)), two cracks L2 and L3 appeared on the

Table 6: The general law of sequestration location of the weak layer affecting the slope slip mode.

Buried depth (m)	10	40	70	99	140
Dip angle (°)	0	8	16	23	32
Sliding mode	Along the weak layer	Along the weak layer	Along the weak layer	Along the weak layer	Along the weak layer

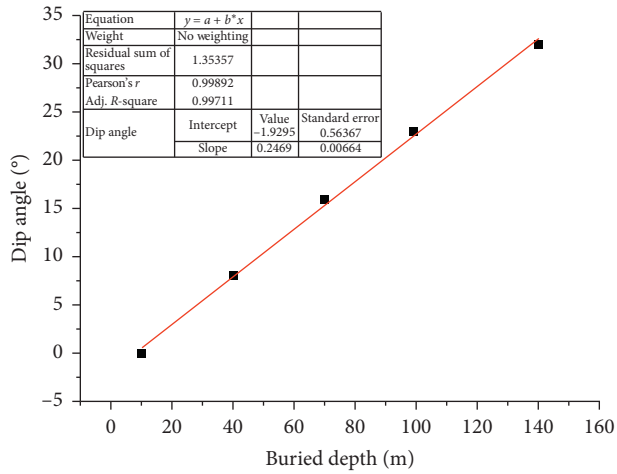

Figure 2: The general law of sequestration location of the weak layer affecting the slope slip mode.

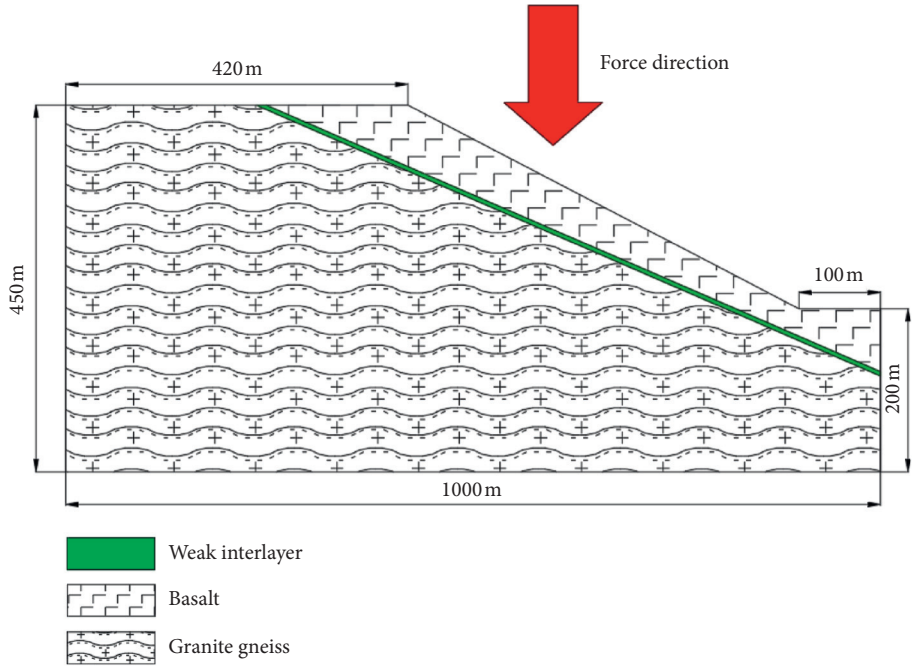

Figure 3: Generalized model section.

Table 7: Mass percentage of each material.

Rock formation	Sand	Lime	Plaster
Granite gneiss	80	12	8
Weak interlayer	—	—	—
Basalt	80	16	4

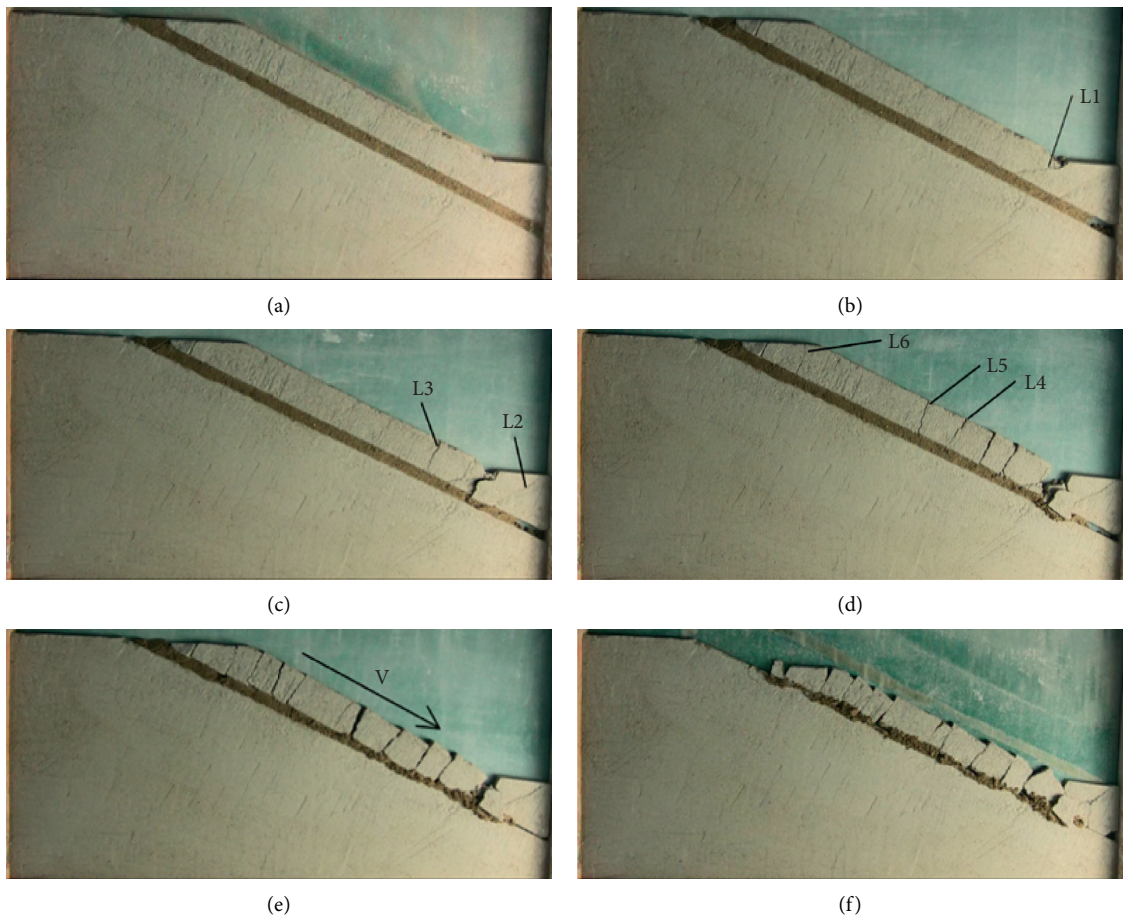

Figure 4: Model break process of experiment 1. (a) Initial state. (b) After 21 s. (c) After 23 s. (d) After 26 s. (e) After 33 s. (f) End of run.

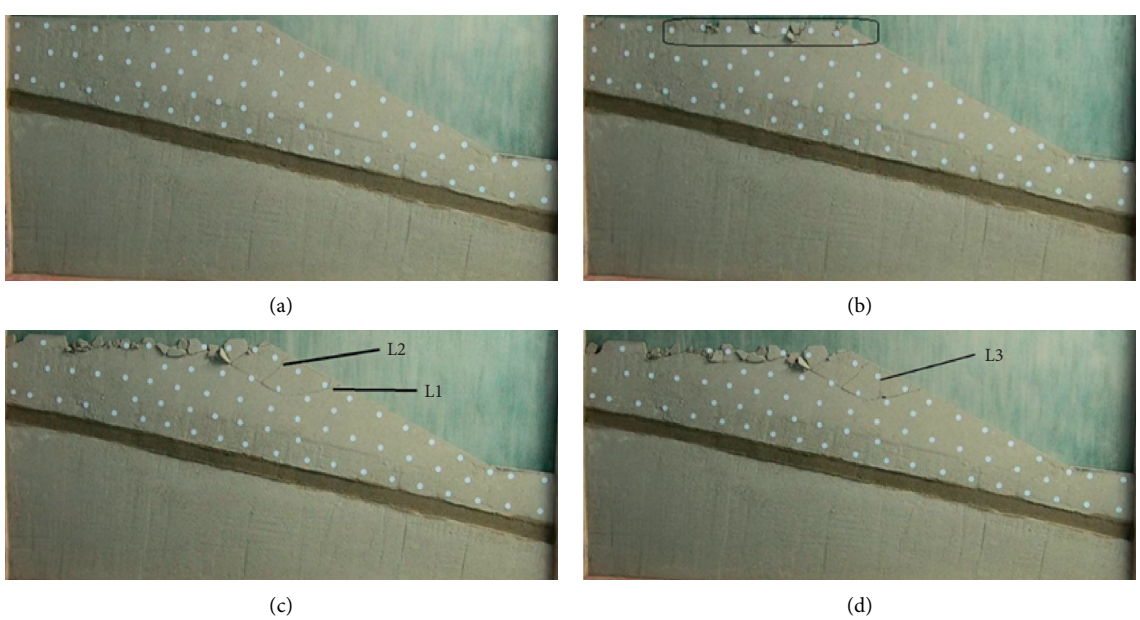

Figure 5: Continued.

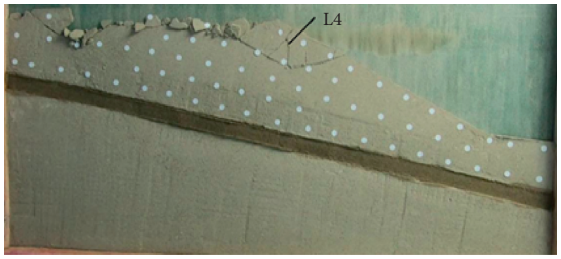

(e)

Figure 5: Model break process of experiment 2. (a) In the beginning. (b) After 15 s. (c) After 23 s. (d) After 27 s. (e) End of run.

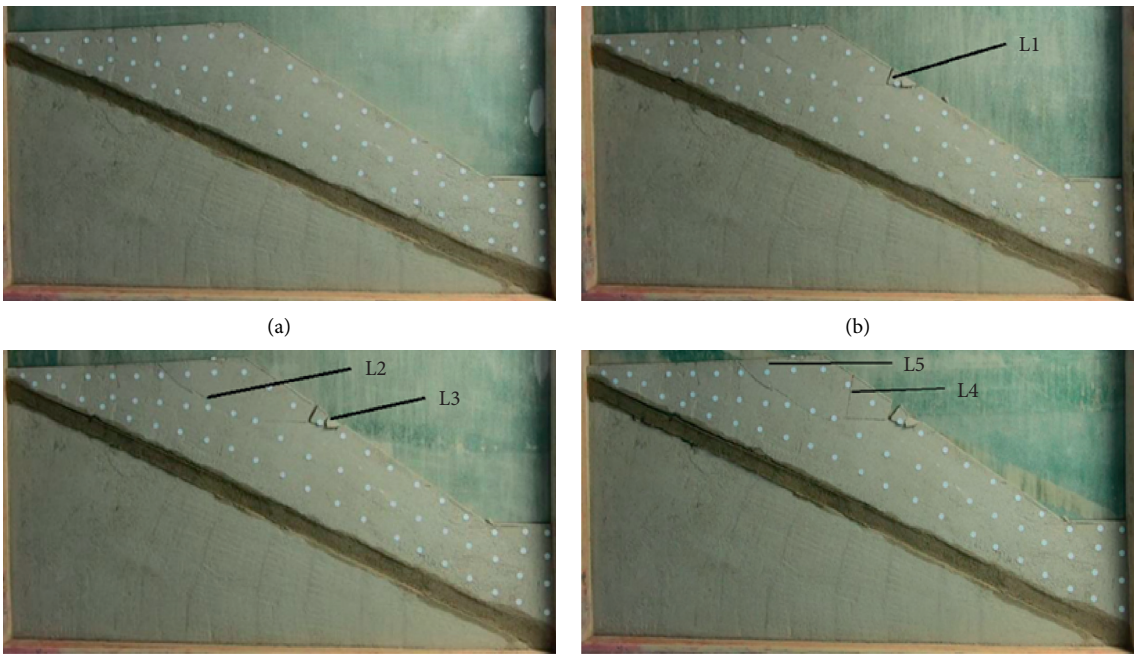

(a) (b)

(c) (d)

Figure 6: Model break process of experiment 3. (a) In the beginning. (b) After 20 s. (c) After 26 s. (d) End of run.

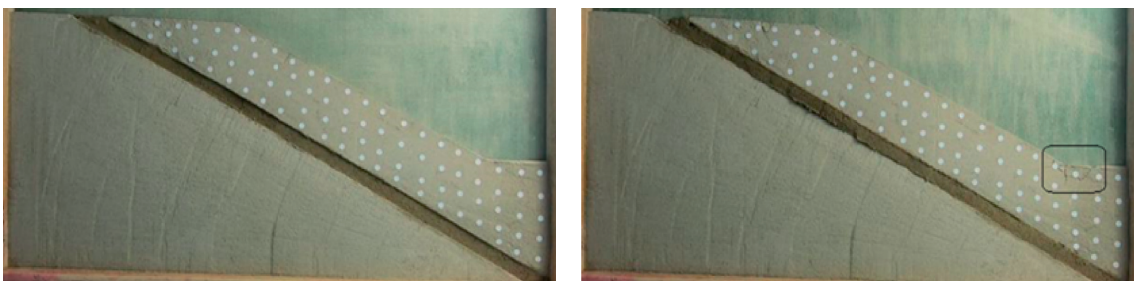

(a) (b)

Figure 7: Continued.

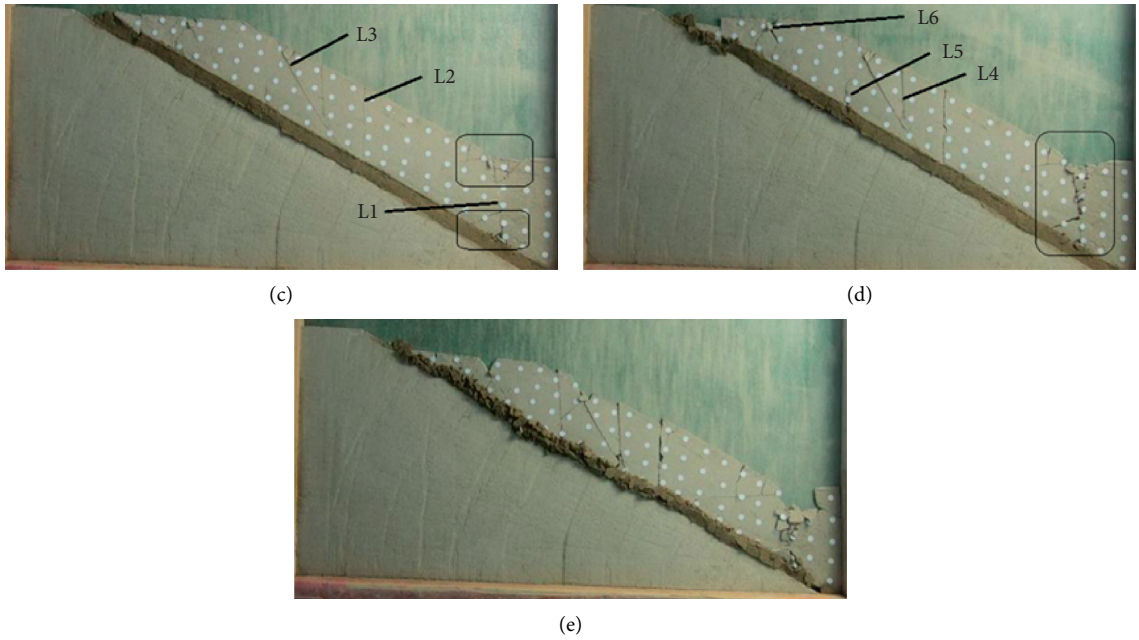

Figure 7: Model break process of experiment 4. (a) In the beginning. (b) After 25 s. (c) After 32 s. (d) After 37 s. (e) End of run.

slope. Crack L2 was arc-shaped and connected to crack L1. The entrance of crack L2 was in the center of the top of the slope, and the exit was in the center of the surface of the slope. L2 cut the slope into an arc-shaped slip surface. Crack L3 appeared in the middle of the small area cut by L1, dividing the small area into two. In the end (Figure 6(d)), new cracks L4 and L5 appeared in the middle of the sliding surface. Both cracks were vertical. The length of L4 was about 8 cm and the length of L5 was about 4 cm. The sliding body was divided into several blocks.

Observing the break process of the model, the break of the slope first started at the slope surface. Small cracks firstly appeared on the slope surface. When the small break area generated, the supporting force of the area at the slope surface is weakened. An arc-shaped failure surface appeared at the slope surface. The bottom friction machine continued to run until the end, and the supporting force on the right side of the arc-shaped failure surface area was weakened. Under the action of gravity, the sliding body lost the support on the right side, and two new cracks appeared, dividing the sliding body into four pieces. From the perspective of the failure process, the failure of the slope is a local small-scale failure, the sliding body on the slope surface has not slipped as a whole, and the slope has no large-scale damage.

3.2.4. Experiment 4: The Dip Angle and the Buried Depth Both Increase (29°, 100 mm). When the buried depth of the weak interlayer increases to 100 mm, the dip angle increases to 29°. The photos of the slope selected at different moments are shown in Figure 7.

Start the bottom friction machine and begin the test. After 25 seconds (Figure 7(b)), the first small-scale damage occurred in the toe of the slope. After 32 seconds (Figure 7(c)), the damage range of the shallow layer at the toe of the slope became larger, and 3 penetration cracks appeared at the toe of the slope and the slope at the same time. Crack L1 appeared at the toe of the slope, which was vertical, about 17 cm long, connected to the first damaged area, and extended to the weak interlayer. There was also a small area of damage in the toe of the slope where the weak interlayer connects with the upper strata. Crack L2 appeared in the center of the slope and was vertical, about 15 cm long. The crack completely penetrated the upper rock layer until it connected with the weak interlayer of the lower layer. Crack L3 appeared in the middle and upper part of the slope and extended to the upper left and was about 22 cm long. The crack also completely penetrated the upper rock layer and was connected to the weak interlayer. After 37 seconds (Figure 7(d)), the cracks at the toe of the slope have completely penetrated the upper and lower areas of the failure of the toe, and the damage range has become larger. Three new through cracks appeared in the upper rock layer. Crack L4 appeared in the middle of the slope and was vertical. It was connected to crack L3, which completely penetrates the upper rock layer and connects to the weak interlayer. Crack L5 appeared at the upper left of crack L3 and was vertical. It completely penetrated the upper rock layer and connected to the weak interlayer. Crack L6 appeared at the top of the slope and is curved upward; it was connected with the weak interlayer. At this time, the upper rock layer of the slope had a tendency to squeeze the weak interlayer, and the upper rock layer had a displacement of about 3 cm in the vertical direction. In the end (Figure 7(e)), the toe of the slope was completely broken, the slope was densely cracked, and the slope as a whole slid along the weak interlayer to the toe, and the slope was eventually destroyed.

Judging from the break process of the slope, the first place where the slope was damaged was at the toe of the slope. Large-scale damage occurred at the toe of the slope first, and then cracks occurred at the slope. The uneven settlement of the weak interlayer resulted in vertical cracks at the toe of the slope. Then, under the action of gravity, the rock strata at the slope surface was pulled apart and slid down along the weak interlayer under the action of gravity. When the slope fails, it slides downward as a whole, and its failure mode is in good agreement with the calculation results of the limit equilibrium method.

4. Conclusions

In this paper, the limit equilibrium method is used to study the relationship between the safety factor and sliding mode of the slope and the sequestration of the weak interlayer in the slope. When the dip angle decreases and the buried depth increases, the safety factor will increase. The sliding mode of the slope follows the rule illustrated in Figure 2. If the point of dip angle and buried depth are at the top left of the line, the slope will break along the weak layer. Otherwise, the slope will break in the shallow part.

The bottom friction experiment verifies the results of limit equilibrium method. In experiments 1 and 4, the slope breaks along the weak interlayer. In these two experiments, the point decided by the sequestration location of the weak interlayer is at the top left of the line in Figure 2. According to the result of limit equilibrium method, the slope will break along the weak interlayer, the same as the experiment. Experiments 2 and 3 also show the same results as the limit equilibrium method, as expected.

Data Availability

The data used to support the findings of this study are available from the corresponding author upon request.

Conflicts of Interest

The authors declare that they have no conflicts of interest regarding the publication of this paper.

Acknowledgments

The authors wish to acknowledge the financial support from the National Key Research and Development Plan (Grant no. 2017YFC1503103).

References

[1] K. Sang, "Statistics and analysis of landslide disaster data in China in the past 60 years," *Technology Communication*, vol. 10, pp. 154–159, 2013.

[2] S. W. Sloan, "Geotechnical stability analysis," *Géotechnique*, vol. 63, no. 7, pp. 531–571, 2013.

[3] L. Q. Li, S. X. Luo, W. K. Wei et al., "Model test study on the influence of rainfall infiltration on the behavior of bedding rock slopes with weak interlayers," *Chinese Journal of Rock Mechanics and Engineering*, vol. 32, no. 9, pp. 1772–1778, 2013.

[4] Z. Z. Liu, L. T. Fa, N. Ma et al., "Influence of hydraulic characteristics of broken zone on slope stability of dagushan iron mine," *Metal Mine*, vol. 7, pp. 56–58, 2012.

[5] Z. C. Li, *Research on the Sliding Mechanism and Landslide Failure Time Prediction and Prediction of the South Side Landslide in Fushun West Open-Pit Mine*, Jilin University, Changchun, China, 2017.

[6] Z. Q. Sun and J. T. Li, "Study on open-pit mine slope stability based on improved TOPSIS method," *IOP Conference Series: Earth and Environmental Science*, vol. 781, no. 2, 2021.

[7] X. L. Liu and D. P. Zhou, "Stability evaluation of rock slope with weak interlayer," *Journal of Southwest Jiaotong University*, vol. 4, pp. 382–386, 2002.

[8] B. T. Xu, C. H. Yan, H. Y. Chen et al., "Experimental study on the mechanical characteristics of weak intercalation of slope rock mass," *Rock and Soil Mechanics*, vol. 11, pp. 3077–3081, 2008.

[9] D. Z. Kong, S. J. Pu, Z. H. Cheng et al., "Coordinated deformation mechanism of the top coal and filling body of gob-side entry retaining in a fully mechanized caving face," *International Journal of Geomechanics*, vol. 21, no. 4, Article ID 04021030, 2021.

[10] W. X. Chen and W. Y. Yu, "The influence of weak interlayer on the stability of open-pit mine slope," *Inner Mongolia Coal Economy*, vol. 2, pp. 30–51, 2016.

[11] G. Behzad, "Unsaturated hydraulic conductivity in dual-porosity soils: percolation theory," *Soil and Tillage Research*, vol. 212, 2021.

[12] C. Chen and J. Zhang, "Experimental study on bottom surface friction model of slope deformation and failure of dumping site with inclined basement," *Metal Mine*, vol. 10, pp. 150–154, 2016.